

**Comparison of an isotopic AGCM with new quasi global satellite
measurements of water vapor isotopologues**

Kei Yoshimura^{1,2}, Christian Frankenberg³, Jeonghoon Lee⁴,
Masao Kanamitsu⁵, John Worden³, and Thomas Röckmann⁶

1: Atmosphere and Ocean Research Institute, University of Tokyo

2: Institute of Industrial Science, University of Tokyo

3: Jet Propulsion Laboratory, NASA

4: Korea Polar Research Institute

5: Scripps Institution of Oceanography, University of California San Diego

6: Institute for Marine and Atmospheric Research Utrecht

Corresponding author:

Kei Yoshimura (kei@aori.u-tokyo.ac.jp),

5-1-5 Kashiwanoha, Kashiwa, Chiba 277-8568, Japan

ABSTRACT

We performed an intensive comparison of an isotope-incorporated atmospheric general circulation model with vapor isotopologue ratio observation data by two quasi global satellite sensors in preparation for data assimilation of water isotope ratios. A global IsoGSM simulation nudged toward the reanalysis wind field, atmospheric total column data from SCIAMACHY on Envisat, and mid-tropospheric (800 to 500 hPa) data from TES on Aura were used. For the mean climatological δD of both the total atmospheric column and the mid-troposphere layer, the model reproduced their geographical variabilities quite well. There is, however, some degree of underestimation of the latitudinal gradient (higher δD in the tropics and lower δD in mid-latitudes) compared to the SCIAMACHY data, whereas there is generally less disagreement except lower δD over the Maritime Continent compared to the TES data. It was also found that the two satellite products have different relationships between water vapor amount and isotopic composition. Particularly, atmospheric column mean δD , which is dominated by lower tropospheric vapor, closely follows the fractionation pattern of a typical Rayleigh-type "rain-out" process, whereas in the mid-troposphere the relationship between isotopic composition and vapor amount is affected by a "mixing" process. This feature is not reproduced by the model, where the relationships between δD and the vapor are similar to each other for the atmospheric column and mid-troposphere. Comparing on a shorter time scale, it becomes clear that the data situation for future data assimilation for total column δD is most favorable for tropical and subtropical desert areas (i.e., Sahel, southern Africa, mid-eastern Asia, Gobi, Australia, and southwest US), whereas the available mid-tropospheric δD observations cover wider regions, particularly over tropical to sub-tropical oceans.

1. Introduction

Stable isotope ratio ($\delta^{18}\text{O}$ and δD) in water has been used not only as proxy information for paleoclimate reconstruction [*Dansgaard et al.*, 1969], but also as a natural tracer for hydrological cycles since the 1960s [*Dansgaard*, 1964]. Largely due to the isotope effects involved in phase changes of water, geographic and temporal variations of isotope ratios emerge in water vapor and precipitation. By using the isotope information in precipitation and vapor, one can study atmospheric vapor cycling processes on various scales, such as large-scale transport and in-cloud processes. Thus, the relationship between atmospheric processes and isotope information in water vapor and precipitation has been intensively studied (e.g., *Craig and Gordon* [1965]; *Ehhalt* [1974]; *Jouzel* [1986]; *Gedzelman and Arnold* [1994]; *Webster and Heymsfield* [2003]; *Yoshimura et al.* [2003; 2004]; *Worden et al.* [2007]).

However, the very small amount of isotopic measurements compared to more "traditional" meteorological data (e.g., wind, water vapor, precipitation, and temperature) has greatly limited research. Though observations of precipitation isotopologues over land at time-scales of a day to a month have been accumulated (e.g., *Welker* [2000]; *Kurita et al.* [2004]; *Bowen* [2008]), there are few precipitation isotope ratio observations over the ocean. Moreover, until recently observations of the isotope ratio of water vapor were severely lacking because traditional isotope measurement techniques are very complicated (e.g., the cryogenic method).

Recent advances in remote sensing observations of water vapor isotopologue ratios via satellites have dramatically increased the number of observed data. *Zakharov et al.* [2004] retrieved the first latitudinal climatology for total column integrated water vapor δD values using the IMG (Interferometric Monitor for Greenhouse gases sensor) sensor on ADEOS. *Worden et al.* [2006] retrieved free tropospheric water vapor δD over tropical regions with

fine temporal and spatial resolution using the TES (Tropospheric Emission Spectrometer) instrument on Aura. *Payne et al.* [2007] and *Steinwagner et al.* [2007; 2010] retrieved a global stratospheric δD distribution on a monthly basis using MIPAS (the Michelson Interferometer for Passive Atmospheric Sounding) on Envisat. *Frankenberg et al.* [2009] derived atmospheric total column δD values from SCIAMACHY measurements (Scanning Imaging Absorption Spectrometer for Atmospheric Cartography) on Envisat. Although limitations still exist in terms of spatial and temporal coverage, resolution, and accuracy, these observations have engendered greater understanding of the basic distribution of water isotopologues and the physical process that drives them. It is also worthwhile to mention that remote sensing with ground-based Fourier Transform Spectroscopy sensors has provided a useful and highly interesting new dataset (e.g., *Schneider et al.* [2010]). Furthermore, in the very recent past, precise optical analyzers for in-situ HDO measurements have become available and will provide a wealth of information in the future (e.g., *Lee et al.* [2006]; *Welp et al.* [2008]).

On the other hand, isotope-incorporated atmospheric general circulation models (AGCM) (*Joussaume et al.* [1984]; *Jouzel et al.* [1987]; *Hoffmann et al.* [1998]; *Mathieu et al.* [2002]; *Noone and Simmonds* [2002]; *Schmidt et al.* [2005]; *Lee et al.* [2007]; *Yoshimura et al.* [2008]; *Tindall et al.* [2009]; *Risi et al.* [2010b]; *Ishizaki et al.*, [submitted]) offer a different approach to understanding isotope ratio distribution. They combine the physical processes associated with isotope ratio changes with dynamic and moist thermodynamic processes of the atmosphere. These models simulate the time evolution of the three-dimensional structure of water vapor isotope ratio distribution with explicit consideration of complex water phase changes associated with moist physical processes in the global atmosphere. Most of the models' results generally match well with the precipitation isotope ratio observations for continental and monthly scales. For vapor isotope ratios however, the models are inconsistent [*Noone and Sturm*, 2010], and an intensive

comparison with observations has not been made due to the lack of sufficient data except *Schmidt et al.*, [2005].

As an advanced effort of the modeling approach, *Yoshimura et al.* [2008] (hereafter Y08) ran an isotope-AGCM applying spectral nudging toward real atmospheric dynamics using the NCEP/DOE Reanalysis (R2; *Kanamitsu et al.* [2002]) dataset. This procedure mimics an isotope data assimilation, but without any observed isotope information. The global simulation forced by reanalysis better reproduced the isotope ratio variations in precipitation for a wide range of time scales from daily to inter-annual. This improvement by the nudging technique was confirmed by subsequent studies (e.g., *Risi et al.* [2010b]).

In this paper, we validate various aspects of the Y08 isotope-AGCM historical simulation using newly published satellite δD products from SCIAMACHY [*Frankenberg et al.*, 2009] and TES [*Worden et al.*, 2007]. This is a further step towards potential data assimilation of water vapor isotope ratios and the production of objective analysis fields of isotope ratios, which have never yet been achieved. In the next section, the model simulation and the satellite-based products are described. The third section compares the results. A summary and conclusions follow.

2. Data and Method

a. SCIAMACHY δD data

In *Frankenberg et al.* [2009], δD in the entire atmospheric column was measured for the first time by the SCIAMACHY grating spectrometer onboard the European research satellite Envisat. In a wavelength window ranging from 2355 to 2375 nm, simultaneous retrievals of HDO and H₂O vertical column densities are enabled. Due to the relatively high detector noise of SCIAMACHY in the short-wave infrared channel 8, the single measurement

noise (1-sigma precision error) in δD is typically 40-100 ‰, depending on total water column, surface albedo and viewing geometry. This error can be significantly reduced by averaging multiple measurements, and the averaging procedure will be described below. The footprint of each measurement is 120 km by 30 km. The retrieval period for this study is 2003 through 2005, in which a total of about 1.9 million scenes are included and the measurement values of δD are systematically and arbitrarily decreased by 20 ‰ to minimize the large scale difference to the model and focus on the spatio-temporal variations only. More details about the retrieval procedure can be found in *Frankenberg et al.* [2009]. Most noteworthy in regard to this study is the fact that SCIAMACHY measurements are performed in the short-wave infrared, thereby exhibiting sensitivity for the entire atmospheric column, including boundary layer water vapor.

b. TES δD data

TES on the Aura satellite is an infrared Fourier transform spectrometer that measures the spectral infrared (IR) radiances between 650 cm^{-1} and 3050 cm^{-1} in limb-viewing and nadir (downward looking) modes. The observed IR radiance is imaged onto an array of 16 detectors that have a combined horizontal footprint of 5.3 km by 8.4 km in the nadir viewing mode. In the nadir view, TES estimates of atmospheric distributions provide vertical information of the more abundant tropospheric species such as H_2O , HDO, O_3 , CO, and CH_4 [Worden et al., 2006]. Simultaneous profiles of HDO and H_2O are obtained from TES thermal infrared radiances between $1,200$ and $1,350\text{ cm}^{-1}$ (7400 to 8300 nm in wavelength) using maximum a posteriori optimal estimation [Worden et al., 2006]. This approach allows for a precise characterization of the errors in the ratio ($[\text{HDO}]/[\text{H}_2\text{O}]$) and its vertical resolution. For this analysis, mean values of the isotopologue ratio (δD) are calculated from averages of $[\text{HDO}]$ and $[\text{H}_2\text{O}]$ between 550 and 800 hPa, where the estimated profiles of δD are most

sensitive. This average has a typical accuracy of 10‰ in the tropics and 24‰ at the poles. Profiles of atmospheric and surface temperature, surface emissivity, effective cloud optical depth and cloud top height are also estimated from TES radiances and are used to stratify δD analysis. A bias in the established HDO spectroscopic line strengths requires a special correction depending on its averaging kernel so that the degree of bias correction varies by each observation [Worden *et al.*, 2011]. The bias correction accounts for the a priori constraint and vertical resolution of the HDO and H₂O profile retrieval. In this study, the retrieval period is 2004 through 2008, in which a total of about 670,000 scenes are included, and the measurement values of δD are systematically and arbitrarily increased by 20 ‰ to minimize the difference to the model field over 45°S-45°N.

c. Common shortcomings of the both satellite data and future direction

Here we should mention that neither TES nor SCIAMACHY are dedicated isotope instruments and that there exist systematic errors [Worden *et al.*, 2007; Frankenberg *et al.*, 2009]. For example, at higher latitudes (particularly poleward of 45°) the retrievals are very close to the a priori assumptions, which are likely erroneous. Furthermore, validations of these satellite products have been difficult due to lack of in-situ measurements and difficulty in data handling. Therefore, the mismatches between the satellite measurements and the model, which are going to be discussed in the later parts of the paper, are not necessarily only due to model errors. As a first step in the improvement of both the satellite instruments and the model, however, it is necessary to reveal the agreement and disagreement between them and to understand their driving mechanism.

For validating the satellite retrievals, there are some on-going activities. Very recent paper of Worden *et al.* [2011] estimated the bias of TES by comparison to dedicated in-situ measurements at Mauna Loa. Schneider and Hase [2011] reported on δD measurement by

IASI (Infrared Atmospheric Sounding Interferometer) data with a higher temporal and spatial resolution than SCIAMACHY and TES, with measurement starting from 2007. Furthermore, the future TROPOMI instrument (TROPospheric Monitoring Instrument; [Levelt, 2008]) will provide HDO/H₂O retrievals in a manner similar to SCIAMACHY but with a greatly improved precision and temporal and spatial sampling frequency. Similar algorithm of SCIAMACHY is applicable to an FTS (Fourier Transform Spectrometer) on the Japanese CO₂ monitoring satellite GOSAT (Greenhouse gases Observing SATellite) (Frankenberg, private communication). In addition, there is the recently started project MUSICA (Multi-platform remote Sensing of Isotopologues for investigating the Cycle of Atmospheric water, <http://www.imkasf.kit.edu/english/musica>). It aims on a consistent on a consistent δD dataset applying ground- and space-based remote sensing as well as surface and aircraft in-situ measurement techniques.

d. Isotope General Circulation Model simulation

The Isotope-incorporated Global Spectral Model (IsoGSM) was developed by Y08 and a 30-year simulation with a global spectral nudging technique [Yoshimura and Kanamitsu, 2008] was performed (data available at <http://hydro.iis.u-tokyo.ac.jp/~kei/IsoGSM1>). The spatial and temporal resolution of the IsoGSM simulation atmospheric output is 2.5°x2.5° and 6 hourly. In this study, this nudged simulation data is used for comparisons with the satellite measurements. In this method, the large scale dynamical forcing was taken from NCEP/DOE Reanalysis 2 [Kanamitsu *et al.*, 2002], and water isotope ratios were fully predicted, including their sources and sinks, without utilizing any water isotope observations. Several validation studies of this model product against limited observations showed that the analysis is sufficiently accurate for various process studies (e.g., Uemura *et al.* [2008]; Abe *et al.* [2009]; Schneider *et al.* [2010]; Berkelhammer *et al.* [2011]).

We prepare a further experiment to examine the sensitivity of the results to the “equilibrium fraction ε ,” which is the degree to which falling rain droplet equilibrates with the surroundings. This parameter is very important to the isotopic exchange between falling droplet and ambient vapor (*Hoffmann et al.* [1998]; *Lee and Fung* [2008]; *Yoshimura et al.* [2010]). It is the essential reason precipitation isotope ratios only reflect the near surface vapor even though the condensation takes place at a much higher atmospheric level. The experiment using the smaller equilibrium fraction of 10% for convective precipitation is called E10 hereafter, whereas the control run (CTL) used an equilibrium fraction of 45%. This decrease of the parameter indicates that a rain drop in a convective cell would less isotopically interact with the ambient vapor than previously thought. The simulation period of E10 with the same nudging scheme starts from 2000, so that the impact of the initial state is sufficiently dissolved for the analysis period of 2003-2007.

With a similar purpose, *Lee et al.* [2009] conducted sensitivity tests to quantify the impact of the timescale for consumption of convective available potential energy (CAPE) on the isotopic distribution. We chose a different way to change a parameter which influences the stable water isotope ratios only similar to *Lee and Fung* [2008] and *Field et al.* [2010], since we want rather not to modify the convective process itself, since the convective process has been long tested, and moreover, it influences the general circulation itself.

e. Processing of the Data

From the IsoGSM simulation results, the nearest location and time of each satellite measurement are extracted for both SCIAMACHY and TES data (hereafter the process is called "collocation"). Thus there is no representativeness difference between the model and the data. The extraction process for SCIAMACHY data is different from that for TES. Since a single measurement by SCIAMACHY has a larger random error [*Frankenberg et al.* 2009],

we average multiple measurements that have been collected for a grid of $2.5^\circ \times 2.5^\circ$ in 6 hours, whereas no averaging of multiple measurements is taken into account for the TES-IsoGSM collocation. We set the threshold value for the averaging as 10. Therefore, the average of the SCIAMACHY measurements is only considered for comparison with IsoGSM if the measurements were made more than 10 times inside a cell of $2.5^\circ \times 2.5^\circ$ for 6 hours. After this procedure, the amount of comparable data shrinks to about 50000, mainly covering the desert regions because of the high IR reflectivity and absence of clouds there [Frankenberg *et al.* 2009].

Because there is some degree of vertical sensitivity regarding the averaging kernels (AK) of the satellite sensors' retrieval algorithms particularly apparently for the TES data, we have applied the AK for each collocated data for TES and calculated the mean δD values for 800-500 hPa level, whereas we have simply extracted the mean δD values in the vapor contents of the total atmospheric column for SCIAMACHY. The application of the TES AK suggested by Lee *et al.* [2011] is written as follows:

$$\mathbf{X}_{GCM}^{New} = \mathbf{X}_a + \mathbf{A}_{TES} [\mathbf{X}_{GCM} - \mathbf{X}_a]$$

$$\mathbf{X} = \begin{bmatrix} \ln(q_{D(1)}) \\ \vdots \\ \ln(q_{D(25)}) \\ \ln(q_{H(1)}) \\ \vdots \\ \ln(q_{H(25)}) \end{bmatrix} \quad \mathbf{A}_{TES} = \begin{bmatrix} \mathbf{A}_{DD} & \mathbf{A}_{DH} \\ \mathbf{A}_{HD} & \mathbf{A}_{HH} \end{bmatrix}$$

where $q_{D(k)}$ and $q_{H(k)}$ are volume mixing ratio of HDO and H_2O , respectively, at TES vertical level k up to 25th level (100hPa), and suffixes of a and GCM indicate a priori assumption and IsoGSM result, respectively. A_{TES} is the averaging kernel matrix of TES.

The TES's AK vary in time and space and TES is less sensitive where there is little water vapor, such as at high latitudes. With the low sensitivity, the retrieval results tend to be close to the a priori assumption, which is why TES sees a smaller latitudinal gradient and

smaller seasonal cycles at high latitudes [Worden *et al.*, 2006]. On the other hand, SCIAMACHY's AK do not vary in time and space. It should be noted that this study first applied TES AK at each single observation occurrence, whereas the previous studies did for time averages such as monthly climatology [Lee *et al.* 2011; Risi *et al.*, submitted]. Thus, the use of the nudged simulation is essential for this study.

3. Results

a. Comparison of annual and seasonal climatology

In Figure 1, the annual mean climatology of the SCIAMACHY measurement (Fig.1a) and the collocated IsoGSM simulations (Fig.1b and 1d) are shown. IsoGSM is a state-of-the art model that captures the general two-dimensional isotopic distribution well. The common maxima over central Africa and the Amazon are likely due to the impact of evapotranspiration from the land surface, leading to isotope enrichment. Over these regions, the "continental effect" is weaker than over mid- and high latitudes as shown in *Frankenberg et al.* [2009]. It is important to note that the annual averages shown in these figures are biased towards specific seasons because the observation frequency depends on many factors, such as minimum signal-to-noise-ratio, cloud cover, or thresholds on solar zenith angles (resulting in less measurement at high latitudes where snow cover and high solar angles reduce the signal level in the shortwave infrared). Whereas this must be taken into account when interpreting the data, it does not affect the model-data comparison because of the collocation.

Despite the qualitatively good agreement, there are also some discrepancies, and the most obvious difference is that the simulated latitudinal isotope gradient is smaller than in the observations. These differences between the model and SCIAMACHY observations are shown in Figure 1c and 1e and they reveal that compared to SCIAMACHY, both experiments

in IsoGSM underestimate the tropical δD values whereas they overestimate sub-tropical δD . The difference between the two experiments (Figure 1b and 1d) is relatively smaller, indicating that the impact of the equilibrium fraction factor ϵ is not as sensitive at the atmospheric column as at the middle troposphere (will be shown in Figure 2).

In Figure 2, the geographical comparisons between the TES data and the collocated and AK-applied IsoGSM results are shown in a similar manner. As for the SCIAMACHY results, the spatial pattern is qualitatively well simulated by both experiments (Fig.2a, 2b, and 2d). Without application of AK, the model overestimates the latitudinal gradient (figure not shown), but such overestimation is corrected by AK application. This might be partly because the TES sensitivity declines at increasing latitudes so that the retrieved values become closer to the a priori, in turn damping both the seasonality and the latitudinal gradients. Moreover, there are large underestimations over the Maritime Continent and Central America as illustrated in Figure 2c, where convective precipitation is most significant. The reason for this big discrepancy will be discussed below.

In Figure 2d and 2e, we compare the E10 results with the satellite retrievals. The impact of changing the equilibrium fraction is apparent over the Maritime region where the discrepancy in the control run was large. The large change in the mid-tropospheric vapor δD is compensated by the changes in precipitation (figure not shown) and surface vapor δD (difference between Figure 1b and 1d) due to the mass balance, but the compensated changes are smaller because of the larger amount of water at near surface or in precipitation than at mid-troposphere. This result is consistent with what *Field et al.* [2010] obtained in their model.

Figure 3 illustrates zonal and tropical averages of SCIAMACHY and IsoGSM data for annual, JJA and DJF climatology. The zonal averages (Figure 3a to 3c) again highlight the model's underestimation of the latitudinal gradient in vapor δD (less enrichment at the tropics and over-enrichment elsewhere). The tropical underestimation is largest in the DJF season.

More detailed information about the origin of the mismatch in the tropics can be obtained by examining the longitudinal variations in the 30°S to 30°N latitudinal belt as illustrated in Figure 3d to 3f. The model's underestimation is larger in the eastern half of the tropics (Figure 3d). The JJA longitudinal variation (Figure 3e) is reasonably reproduced by the model, but the model misses the significant enrichment in the 20°W to 20°E region, which corresponds to the tropical African region (around 10°S-10°N). This implies that the model misses an important process of isotope enrichment in this region, if the SCHIAMACHY data is trustable enough. Though it is rather wet region, more intensive vapor recycling process (e.g., *Numaguti, [1999]*) would have been taken into account than the model simulates. The DJF tropical zonal variation (Figure 3f) is poorly simulated, and discrepancy between the model and the satellite seems larger in the eastern half of the tropical band. This larger discrepancy for δD strongly contributes to the annual average over the eastern half. The sensitivity run E10 consistently increased the δD of vapor because of the reduced isotopic exchange between falling droplets and ambient vapor. The global average of the increase was about 6 ‰, and slightly larger at the tropics. Nevertheless, the strong longitudinal variability of the measurements in the winter months is still not captured by the model.

Figure 4 is similar to Figure 3, but for the TES data. Furthermore, IsoGSM results without AK application are also shown. Without AK, the model-data difference becomes particularly large poleward of 45°, where TES's degrees of freedom for the retrieval of the δD is substantially smaller than 1 [*Worden et al., 2006*]. With AK, this difference is dramatically resolved. However due to the erroneous feature at high latitudes mentioned before, we do not further interpret the high latitude data. Equatorward of 45°, however, the model's latitudinal gradient matches the observations reasonably well both with and without AK application. For the tropical longitudinal variations (Figure 4d to 4f), the model follows the large-scale patterns much better than for the SCHIAMACHY data. In general, the model overestimates the depletion between 100°E and 180° which corresponds to the Maritime Continent and

surrounding oceans. This feature was previously noted in the description of Figure 2c. The amplification of the strong depletion is reduced for DJF (Figure 4f), and the overall match becomes better than that of JJA. As a result of averaging over the entire year, the annual latitudinal variation of CTL is slightly over-amplified in the model (Figure 4d). However, this erroneous feature is partly fixed by the E10 experiment, particularly over the Maritime Continent and surrounding oceans at JJA. The smaller equilibrium fraction increased the δD of mid-tropospheric vapor by up to 30‰, a much larger amount than that of the total atmospheric column vapor as previously noted.

In Figure 5, scatter diagrams between the satellites' observation climatologies and the IsoGSM simulation climatology are shown. This time only the E10 result is shown because of the better match towards the satellite data. Figure 5a to 5c shows that the distribution pattern is reasonably well simulated with a correlation coefficient (R) of 0.78~0.81. As discussed above, the range of the IsoGSM's spatial and temporal distribution in atmospheric column δD is smaller than that of SCIAMACHY by a factor of 0.49~0.50 (i.e., $\sigma_{sim}/\sigma_{obs}$). On the contrary, the mid-tropospheric δD is simulated with a slightly larger variance for spatial distribution compared to the TES observation, by a factor of 0.83~0.94 with a correlation coefficient of 0.76~0.84, as shown in Figures 5d to 5f. It should be noted that the distinctive area of the larger discrepancy in the TES comparison is still visible, particularly in Figure 5e. This is derived from the model's underestimation of δD over the Maritime Continent and Central America compared to TES, as mentioned above, whereas the discrepancy was much larger in the CTL experiment.

The general comparisons of correlation coefficients and slopes between the model simulations and the data are not very time sensitive. Figure 5b and 5c show the relationships for JJA and DJF, respectively, for total atmospheric column δD with SCIAMACHY data, and Figure 5e and 5f show the same for mid-tropospheric δD with TES data. The area of the biggest discrepancy between TES and IsoGSM is more apparent in JJA than DJF, which is

probably due to the more active convective precipitation over the mismatched regions in summer.

b. Relationship between vapor amount and δD

Figure 6 presents relationships between water vapor amount (volume mixing ratio or VMR in ‰) and its δD in the satellite observations and the simulation over tropical to mid-latitude regions (45°S to 45°N). Both axes are in logarithmic representation; i.e., the vertical axis is $\log(\delta D + 1)$, and the horizontal axis is \log of VMR, so that a typical Rayleigh distillation process should form a straight line whose slope equals the fractionation factor α minus 1. Figure 6a to 6c, in which both the SCIAMACHY (blue dots) and TES observations (red dots) are plotted, indicates that the slopes of the linear regressions in SCIAMACHY are steeper than those of TES. However, these slopes (0.056~0.068 for SCIAMACHY and 0.021~0.038 for TES) are all smaller than that of a typical Rayleigh distillation process line (black solid lines), which should be around 0.08~0.15 depending on ambient temperature (+20~-20°C) (Majoube, 1971a, 1971b). This difference is partly caused by the omission of high latitude regions in both observational datasets, where typically Rayleigh processes dominantly affect the variation of δD . More importantly, the distinct differences between the SCIAMACHY and TES plots imply that surface vapor is more influenced by the Rayleigh-type rainout process, whereas the mid-troposphere vapor is more influenced by mixing of isotopically distinct vapor masses without isotope fractionation. This implication agrees with the previous finding [Galewsky and Hurley, 2010]. Furthermore, there is a negative correlation in the TES plots where VMR is larger than 10‰. This is due to the "amount effect" [Dansgaard, 1964; Lawrence *et al.*, 2004; Lee and Fung, 2008; Risi *et al.*, 2008; Field *et al.*, 2010] over the tropics, where much rain and its vapor are associated with some heavy isotope depletion.

In the model (Figure 6d to 6f), these relationships are differently simulated. First, the negative correlations at high vapor amounts are much more apparent than in the measurements. This feature is particularly distinguishable over the Maritime Continents and it is arguably stated that the amount effect associated with convective process is to some extent overestimated in the model. Second, the slopes of the linear regression lines for atmospheric column vapor (0.011~0.037) became similar to those for mid-troposphere (0.019~0.031), whereas the satellite observations showed the steeper slopes for SCIAMACHY than TES. Third, these simulated values for the SCIAMACHY observation have much shallower slopes than the observation, whereas both of the slopes are more similar for TES.

Such an analysis of the slope ($\alpha-1$) has been discussed in *Schneider et al.* [2010] at two ground sites. In their results (Figure 7 in *Schneider et al.* [2010]), the slope is higher at surface and decreased with height. This relationship is consistent in the TES/SCIAMACHY comparison, even though their analysis is based on temporal variability whereas ours is on spatial variability. The consistent results are obtained in the model too, i.e., the slope tends to stay unchanged (at subtropics) or slightly increased (at subarctic).

c. Seasonal variations in vapor δD

Figures 7 and 8 show 3-year averaged annual cycles of regional means over $30^\circ \times 20^\circ$ (longitude x latitude) regions for SCIAMACHY and TES, respectively. To make the monthly averaged regional means, simple arithmetic averages of all monthly $2.5^\circ \times 2.5^\circ$ data over a $30^\circ \times 20^\circ$ region were used. The respective collocated simulation results of both CTL (green dotted lines) and E10 (red dashed lines) are also shown. In general, the seasonal variations of both satellite datasets are well reproduced by the simulations in most regions.

In comparing the SCIAMACHY and IsoGSM simulations (Figure 7), remarkable

consistency is observable over the 20°N-40°N latitude band. Due to the weaker latitudinal gradient in the model simulation, there are overestimation biases at higher latitudes (>40°N) and underestimation bias at lower latitudes (<20°N). However, the patterns of the seasonal variations are reasonably well reproduced over the Northern Hemisphere in both experiments. In the Southern Hemisphere, however, the reproducibility is not as good. This is partly because the skill of the IsoGSM atmospheric analysis over the SH is not as good as over the NH (Y08). Also, the SCIAMACHY measurements have less credibility over oceans [Frankenberg *et al.*, 2009].

The seasonal variations observed by TES are also reasonably reproduced by IsoGSM over low to middle latitudes (40°S to 40°N), except over the Maritime Continents (20°S-20°N and 90°E-180°) by CTL. As mentioned above, the discrepancy over the Maritime Continents is likely derived from the poor representation of isotopic behavior in convective processes, particularly related to the isotopic exchange process between falling droplets and ambient vapor. E10 shows much better seasonal variation over these regions.

d. Comparison in short-term temporal variations

In Figure 9, the time series of atmospheric column mean δD and TPW (total precipitable water) from SCIAMACHY and the IsoGSM E10 experiment at a specific grid point of 15E and 20N (Sahel region) for the year of 2005 are shown. Since the basic feature is almost the same, the CTL experiment is omitted. As already noted, a single gridded data point from SCIAMACHY is an average of more than 10 single measurements in a 2.5°x2.5° and 6-hour space. Single measurements by SCIAMACHY fluctuate greatly, particularly for δD , as shown by small dots in the figure. However, despite the large range of the fluctuation, the spatio-temporal averages for the vapor δD are reasonably well reproduced by the model (R=0.749). Note that this correlation is calculated using the averaged data for observation,

therefore the random noise by single measurement hardly affected the result. Although it may be necessary to more carefully investigate the systematic and representativeness error characteristics, the good match in variability and sufficient number of valid measurements (N=64) point to promising potential for four-dimensional data assimilation in the future.

Compared to the isotope information, the TPW from the model and measurements match much better ($R=0.882$), with smaller fluctuations from each dataset. Though related via Rayleigh processes, the isotopic composition has independent variability from that of water vapor amount. Consequently the assimilation of the isotope information would give some additional constraint to the model, which may affect the quality of the hydrological cycle and forecasting predictability.

Risi et al. [2010a] shows a similar plot at Niamey (13.52°N 2.09°E) in there Figure 4. They pointed out that the model significantly underestimated the short-term peak-to-peak fluctuations compared to SCIAMACHY. This is somewhat true in this study, too, as the slope of the regression line is 1.54 (Figure 9b), but it seems the IsoGSM shows closer agreement to the satellite data in terms of the amplitudes of short-term variability.

Figure 10 shows similar plots to Figure 9, but for TES at 67.5E and 25N (over the Arabian Sea) for 2006. δD (Figure 10a and 10b) and volume mixing ratio of water vapor (Figure 10c and 10d) of mean middle (800 hPa to 500 hPa) tropospheric air are shown. The 6-hourly model simulation without AK application is shown as reference, too (sky blue lines). Unlike the SCIAMACHY case, there is no spatio-temporal averaging, so that each red dot in the figure represents a single measurement by TES. Though the correlation coefficient is smaller than that of the previous figure for a SCIAMACHY time series, it is a positive correlation between observed and modeled mid-tropospheric δD ($R=0.681$). The amplitude of model variability is slightly larger than that of TES (slope=0.61) even though the TES data does not have any averaging in a grid. This means that compared to the model the TES observations appear to miss some extent of the short-term variability, which could be a

limitation when data assimilation is considered. The volume mixing ratio shows higher reproducibility than δD , similar to SCIAMACHY.

Figure 11 shows two-dimensional maps of correlation coefficients obtained from the comparison of high frequency seasonal variations as in Figures 9 and 10 between SCIAMACHY and the IsoGSM E10 model run (Figure 11a and 11b), and between TES and IsoGSM E10 (Figure 11c and 11d). From the SCIAMACHY figures, it is shown that a valid grid with more than 10 comparable data during 2005 is preferably located in the tropical and subtropical desert areas (i.e, Sahel, southern Africa, middle east Asia, Gobi, Australia, and southwest US). The temporal variability of atmospheric column δD is reasonably reproduced ($R > 0.6$) by the model in these areas (Figure 11a). However, there are also regions of significant mismatch along the east African coast and in South Africa. The correlation coefficients of the TPW are always very high (close to 1) in all areas where data are available (Figure 11b).

TES data covers wider regions, particularly over oceans (Figure 11c and 11d). The correlation coefficients for δD vary for different locations. They have rather low values over the tropics, but higher values towards higher latitude (poleward of 20°) because weather patterns are more controlled by large-scale dynamics than local parameterized processes in the higher latitudes (consistent with [Yoshimura *et al.*, 2003; 2008; Risi *et al.*, 2010b]). The same figure for humidity shows generally larger correlation coefficients, but a similar tendency of low correlations in the inner tropics is observable. This is due to the generally small seasonality in these tropical bands.

Figure 12 shows the slopes of linearly regressed relationships between the model and the satellite data. As partly known in the Figure 9 and 10, for δD , the slope is mostly greater than 1 in SCIAMACHY (Figures 12a) and mostly smaller than 1 in TES (Figure 12c). Interestingly, slopes for humidity are less than 1 for both cases in the large part (Figure 12b and 12d), but in average, similar to correlations, these numbers are closer to 1 than those of

δD . From this figure, it is implicated that there is some potential to give some additional constraint to the model when SCIAMACHY data is assimilated. In case of TES, there could be potential over subtropical regions ($20^{\circ}\sim 40^{\circ}$, where slope is more than 0.8) in both hemispheres, but limited impact could be expected particularly over tropical oceans where the slope is very small (less than 0.4).

4. Summary and Conclusions

In preparation for data assimilation of water isotope information, we have performed an intensive comparison of an isotope-incorporated AGCM with vapor isotopologue ratio observation data by two satellite sensors. A global IsoGSM simulation nudged toward the reanalysis dynamical field, atmospheric column data from SCIAMACHY on Envisat, and mid-tropospheric (800 to 500 hPa) data from TES on Aura were used. The model reproduced the geographical variability of the mean climatological δD of the total atmospheric column and of the mid-troposphere quite well. There is, however, a clear underestimation of the latitudinal gradient (higher δD in the tropics and lower δD in mid-latitudes) compared to the SCIAMACHY data, whereas there is generally less disagreement except lower δD over the Maritime Continent compared to the TES data.

It was found that the two satellite products have different relationships between the water vapor amount and its isotopologue ratio. In many ways, both satellite products are complementary (SCIAMACHY samples total column and is best over the continents whereas TES measures between 500-800hPa and is most reliable over oceans). Particularly, atmospheric column mean δD , which is dominated by lower tropospheric vapor, exhibits a closer relationship with a typical Rayleigh-type "rain-out" process with isotopic fractionation, whereas in the mid-troposphere it is more affected by a "mixing" process. This feature is not quite reproduced by the model, where the relationships between δD and the vapor are similar

to each other for both the atmospheric column and the mid-troposphere, i.e., both are mainly driven by the Rayleigh-type “rain-out” process. The seasonal variations of the vapor δD were generally adequately reproduced by the model, with some exceptions in particular regions. These regions include mid-latitudes in the Southern Hemisphere for atmospheric column δD and the Maritime Continent (20°S-20°N and 90°E-180°) for mid-tropospheric δD . The discrepancy over the Maritime Continent is likely derived from the poor representation of the isotopic behavior in convective processes, and it was slightly improved in the model run where the equilibrium fraction was reduced, which restrains the isotopic exchange between falling droplets and ambient vapor.

Finally, we compared the model and the satellite data on a shorter time scale. We found that for total column δD , SCIAMACHY measurements show larger fluctuations than the model, but both datasets correlate reasonably well. On the contrary for mid-tropospheric δD , the model’s short-term fluctuation range is larger in the mode than for TES measurement. It is clear that the data situation for future data assimilation is best for tropical and subtropical desert areas (i.e, Sahel, southern Africa, middle eastern Asia, Gobi, Australia, and southwestern US) for total column δD , whereas the available mid-tropospheric δD observations cover wider regions, particularly over oceans. However, the measurement precision and sampling frequency of future instruments such as TROPOMI will provide more, and more reliable, total column isotopologue ratio observations. The same is perhaps true with the IASI (Infrared Atmospheric Sounding Interferometer) data, which has a higher temporal and spatial resolution [*Schneider and Hase, 2011*]. However, it must be noted that neither TES nor SCIAMACHY nor TROPOMI nor IASI are dedicated water isotopologue ratio instruments and this product was not an official target when these instruments were designed.

This paper compared two satellite products and a model simulation on various scales in time and space. Some of the discrepancies between the model and the observations found

in this study could be corrected when performing data assimilation, which may lead to significant improvement of four-dimensional analyses of water isotope ratio distribution, which in turn would provide us with information to investigate further details of atmospheric hydrologic cycles. It is of prime importance to more understand the uncertainties of the satellite data.

Acknowledgments:

A part of this research was funded by the Japan Society for the Promotion of Science (JSPS) Grant 23686071. The numerical simulations were performed with computing resources at the Center for Observations and Prediction at Scripps (COMPAS) and at TeraGrid. Part of this work was also funded by the California Energy Commission Public Interest Energy Research (PIER) program, which supports the California Climate Change Center (Award Number MGC-04-04) and NOAA (NA17RJ1231). The views expressed herein are those of the authors and do not necessarily reflect the views of NOAA. We would like to thank Dr. J. Roads for his encouragement in the beginning of this study. The assistance of Ms. D. Boomer in refining the writing is appreciated. Authors thank all the comments from two reviewers including Dr. Matthias Schneider.

REFERENCES

- Abe, O., S. Agata, M. Morimoto, M. Abe, K. Yoshimura, T. Hiyama, and N. Yoshida, 2009: A 6.5-year continuous record of sea surface salinity and seawater isotopic composition at Harbor of Ishigaki Island, southwest Japan, *Isotopes in Environmental and Health Studies*, **45**, 247-258.
- Berkelhammer, M., L. Stott, K. Yoshimura, K. Johnson, and A. Sinha, 2011: Synoptic and mesoscale controls on the isotopic composition of precipitation in the southwestern US, *Clim. Dyn.*, in print.

- Bowen, G. J., 2008: Spatial analysis of the intra-annual variation of precipitation isotope ratios and its climatological corollaries, *J. Geophys. Res.*, **113**, D05113, doi: 10.1029/2007JD009295.
- Craig, H. and L. Gordon, 1965: Deuterium and oxygen-18 variations in the ocean and the marine atmosphere. In *Stable Isotopes in Oceanographic Studies and Paleotemperatures* (ed. E. Tongiorgi), Spoleto, Italy, 9–130.
- Dansgaard, W., 1964: Stable isotopes in precipitation. *Tellus*, **16**, 436-468.
- Dansgaard, W., S. J. Johnsen, J. Møller and C. C. Langway, Jr. 1969: One thousand centuries of climatic record from camp century on the Greenland ice sheet, *Science*, **166**, 377-380.
- Ehhalt, D. H., 1974: Vertical profiles of HTO, HDO and H₂O in the troposphere, Tech. Rep. NCAR-TN/STR-100, Natl. Cent. for Atmos. Res., Boulder, Colo.
- Field, R. D., D. B. A. Jones, and D. P. Brown, 2010: Effects of postcondensation exchange on the isotopic composition of water in the atmosphere, *J. Geophys. Res.*, **115**, D24305, doi:10.1029/2010JD014334.
- Frankenberg, C., K. Yoshimura, T. Warneke, I. Aben, A. Butz, N. Deutscher, D. Griffith, F. Hase, J. Notholt, M. Schneider, H. Schrijver, and T. Röckmann, 2009: Dynamic processes governing the isotopic composition of water vapor as observed from space and ground, *Science*, **325**, 1374-1377, doi: 10.1126/science.1173791.
- Gedzelman, S. D. and R. Arnold, 1994: Modeling the isotopic composition of precipitation, *J. Geophys. Res.*, **99**, 10344-10471.
- Galewsky, J. and J. V. Hurley, 2010: An advection - condensation model for subtropical water vapor isotopic ratios, *J. Geophys. Res.*, **115**, D16116, doi:10.1029/2009JD013651.
- Hoffmann, G., M. Werner, and M. Heimann, 1998: The water isotope module of the ECHAM Atmospheric General Circulation Model – A study on timescales from days to several years, *J. Geophys. Res.*, **103**, 16,871– 16,896.

- Ishizaki, Y., K. Yoshimura, S. Kanae, M. Kimoto, N. Kurita, and T. Oki, 2011: Interannual variability of H₂¹⁸O in precipitation over the Asian monsoon region, submitted to *J. Geophys. Res.*
- Joussaume, S., R. Sadourny, and J. Jouzel, 1984: A general circulation model of water isotope cycles in the atmosphere, *Nature*, **311**, 24–29.
- Jouzel, J. 1986: Isotopes in cloud physics: Multiphase and multistage condensation processes, in Handbook of Environmental Isotope Geochemistry, vol. 2, edited by P. Fritz and J.C. Fontes, pp.61-112, Elsevier, New York.
- Jouzel, J., G. L. Russell, R. J. Suozzo, R. D. Koster, J. W. C. White, and W. S. Broecker, 1987: Simulations of HDO and H₂¹⁸O atmospheric cycles using the NASA GISS general circulation model: The seasonal cycle for present-day conditions, *J. Geophys. Res.*, **92**, 14,739–14,760.
- Kanamitsu, M., W. Ebisuzaki, J. Woolen, J. Potter, and M. Fiorino, 2002: NCEP/DOE AMIP-II Reanalysis (R-2), *Bull. Amer. Meteor. Soc.*, **83**, 1631-1643.
- Kurita, N. Yoshida, G. Inoue, and E. A. Chayanova, 2004: Modern isotope climatology of Russia: A first assessment. *J. Geophys. Res.*, **109**, D03102, doi:10.1029/2003JD003404.
- Lawrence, J. R., S. D. Gedzelman, D. Dexheimer, H.K. Cho, G. D. Carrie, R. Gasparini, C. R. Anderson, K. P. Bowman, and M. I. Biggerstaff, 2004: Stable isotopic composition of water vapor in the tropics, *J. Geophys. Res.*, **109**, D06115, doi:10.1029/2003JD004046.
- Lee, J., J. Worden, D. Noone, K. Bowman, A. Eldering, A. Legrande, J.-L. F. Li, G. Schmidt, and H. Sodemann, 2011: Relating tropical ocean clouds to moist processes using water vapor isotope measurements, *Atmos. Chem. Phys.*, **11**, 741-752.
- Lee, J. -E., I. Fung, D. J. DePaolo, and C. C. Henning 2007: Analysis of the global distribution of water isotopes using the NCAR atmospheric general circulation model, *J. Geophys. Res.*, **112**, doi:10.1029/2006JD007657.
- Lee, J. -E. and I. Fung, 2008: "Amount effect" of water isotopes and quantitative analysis of

- post-condensation processes, *Hydrol. Process.*, **22**, 1-8.
- Lee, J.-E., R. Pierrehumbert, A. Swann, and B. R. Lintner, 2009: Sensitivity of stable water isotopic values to convective parameterization schemes, *Geophys. Res. Lett.*, **36**, L23801, doi:10.1029/2009GL040880.
- Lee, X., R. Smith, and J. Williams, 2006: Water vapor $^{18}\text{O}/^{16}\text{O}$ isotope ratio in surface air in New England, USA. *Tellus*, **58B**, 293–304.
- Levelt, P. F. (Ed), 2008: Final Report of TROPOMI User Workshop, RP-TROPOMI-KNMI-015, 28pp.
- Mathieu, R., D. Pollard, J. E. Cole, J. W. C. White, R. S. Webb, and S. L. Thompson, 2002: Simulation of stable water isotope variations by the GENESIS GCM for modern conditions, *J. Geophys. Res.*, **107**(D4), 4037, doi:10.1029/2001JD 900255.
- Noone, D., and I. Simmonds, 2002: Associations between d^{18}O of water and climate parameters in a simulation of atmospheric circulation 1979–1995, *J. Climate*, **15**, 3150–3169.
- Noone, D., and C. Sturm, 2010: Comprehensive dynamical models of global and regional water isotope distributions. In: *West, J., G. Bowen, T. Dawson and K. Tu (eds.) Isoscapes*, Springer, 195-219.
- Numaguti, A., 1999: Origin and recycling processes of precipitating water over the Eurasian continent: Experiments using an atmospheric general circulation model, *J. Geophys. Res.*, **104**(D2), 1957-1972.
- Payne, V. H., D. Noone, A. Dudhia, C. Piccolo, and R. G. Grainger, 2007: Global satellite measurements of HDO and implications for understanding the transport of water vapour into the stratosphere, *Q. J. R. Meteorol. Soc.*, **133**, 1459-1471.
- Risi, C., S. Bony, and F. Vimeux, 2008: Influence of convective processes on the isotopic composition ($\delta^{18}\text{O}$ and δD) of precipitation and water vapor in the tropics: 2. Physical interpretation of the amount effect, *J. Geophys. Res.*, **113**, D19306,

doi:10.1029/2008JD009943.

- Risi, C., S. Bony, F. Vimeux, C. Frankenberg, D. Noone, and J. Worden, 2010a: Understanding the Sahelian water budget through the isotopic composition of water vapor and precipitation, *J. Geophys. Res.*, **115**, D24110, doi:10.1029/2010JD014690.
- Risi, C., S. Bony, F. Vimeux and J. Jouzel, 2010b: Water stable isotopes in the LMDZ4 General Circulation Model: model evaluation for present day and past climates and applications to climatic interpretation of tropical isotopic records, *J. Geophys. Res.*, **115**, doi:10.1029/2009JD013255.
- Risi, C, et al., 2011: Process-evaluation of tropical and subtropical tropospheric humidity simulated by general circulation models using water vapor isotopic observations, submitted to *J. Geophys. Res.*
- Schmidt, G. A., G. Hoffmann, D. T. Shindell, and Y. Hu, 2005: Modeling atmospheric stable water isotopes and the potential for constraining cloud processes and stratosphere-troposphere water exchange, *J. Geophys. Res.*, **110**, D21314, doi:10.1029/2005JD005790.
- Schneider, M., K. Yoshimura, F. Hase, and T. Blumenstock, 2010: The ground-based FTIR network's potential for investigating the atmospheric water cycle, *Atmos. Chem. Phys.*, **10**, 3427-3442.
- Schneider, M. and Hase, F., 2011: Optimal estimation of tropospheric H₂O and δ D with IASI/METOP, *Atmos. Chem. Phys. Discuss.*, **11**, 16107-16146.
- Steinwagner, J., M. Milz, T. von Clarmann, N. Glatthor, U. Grabowski, M. Höpfner, G. P. Stiller, and T. Röckmann, 2007: HDO measurement with MIPAS, *Atmos. Chem Phys.*, **7**, 2601-2615.
- Steinwagner, J., S. Fueglistaler, G. Stiller, T. von Clarmann, M. Kiefer, P. P. Borsboom, A. van Delden and T. Röckmann, 2010: Tropical dehydration processes constrained by the seasonality of stratospheric deuterated water, *Nature Geosci.*, **3**, 262-266.

- Tindall, J. C., P. J. Valdes, and L. C. Sime, 2009: Stable water isotopes in HadCM3: Isotopic signature of El Niño–Southern Oscillation and the tropical amount effect, *J. Geophys. Res.*, **114**, D04111, doi:10.1029/2008JD010825.
- Uemura, R., Y. Matsui, K. Yoshimura, H. Motoyama, N. Yoshida, 2008: Evidence of deuterium excess in water vapour as an indicator of ocean surface conditions, *J. Geophys. Res.*, **113**, doi:1029.10/2008JD010209.
- Webster, C. R., and A. J. Heymsfield, 2003: Water isotope ratios D/H, $^{18}\text{O}/^{16}\text{O}$, $^{17}\text{O}/^{16}\text{O}$ in and out of clouds map dehydration pathways, *Science*, **302**, 1742– 1745.
- Welker, J. M., 2000: Isotopic ($\delta^{18}\text{O}$) characteristics of weekly precipitation collected across the USA: an initial analysis with application to water source studies. *Hydrol. Process.*, **14**, 1449-1464.
- Welp, L. R., X. Lee, K. Kim, T. J. Griffis, K. A. Billmark, and J. M. Baker, 2008: $\delta^{18}\text{O}$ of water vapour, evapotranspiration and the sites of leaf water evaporation in a soybean canopy, *Plant, Cell & Environment*, **31**, doi: 10.1111/j.1365-3040.2008.01826.x.
- Worden, J., *et al.* 2006: Tropospheric Emission Spectrometer observations of the tropospheric HDO/H₂O ratio: Estimation approach and characterization, *J. Geophys. Res.*, **111**, D16309, doi:10.1029/2005JD006606.
- Worden, J, D. Noone, and K. Bowman, 2007: Importance of rain evaporation and continental convection in the tropical water cycle, *Nature*, **445**, doi:10.1038/ nature05508
- Worden, J., D. Noone, J. Galewsky, A. Bailey, K. Bowman, D. Brown, J. Hurley, S. Kulawik, J. Lee, and M. Strong, 2011: Estimate of bias in Aura TES HDO/H₂O profiles from comparison of TES and in situ HDO/H₂O measurements at the Mauna Loa observatory, *Atmos. Chem. Phys.*, **11**, 4491-4503, 2011.
- Yoshimura, K., T. Oki, N. Ohte, and S. Kanae, 2003: A quantitative analysis of short-term ^{18}O variability with a Rayleigh-type isotope circulation model. *J. Geophys. Res.*, **108**, 4647, doi:10.1029/2003JD003477.

- Yoshimura, K., T. Oki, and K. Ichiyangi, 2004: Evaluation of two-dimensional atmospheric water circulation fields in reanalyses by using precipitation isotopes databases. *J. Geophys. Res.*, **109**(D20), D20109, doi:10.1029/2004JD004764.
- Yoshimura, K., M. Kanamitsu, D. Noone, and T. Oki, 2008: Historical isotope simulation using Reanalysis atmospheric data, *J. Geophys. Res.*, **113**, D19108, doi:10.1029/2008JD010074.
- Yoshimura, K., and M. Kanamitsu, 2008: Dynamical global downscaling of global reanalysis, *Mon. Wea. Rev.*, **136**, 2983–2998.
- Yoshimura, K., M. Kanamitsu, and M. Dettinger, 2010: Regional downscaling for stable water isotopes: A case study of an Atmospheric River event, *J. Geophys. Res.*, **115**, doi:10.1029/2010JD014032.
- Zakharov, V. I., R. Imasu, K. G. Gribanov, G. Hoffmann, and J. Jouzel, 2004: Latitudinal distribution of the deuterium to hydrogen ratio in the atmosphere water vapor retrieved from IMG/ADEOS data, *Geophys. Res. Lett.*, **31**, L12104, doi:10.1029/2004GL019433.

Figure 1: Left column; annual mean climatology of δD in atmospheric vapor for SCIAMACHY (a), collocated IsoGSM CTL experiment (b), and collocated IsoGSM E10 experiment (d). Right column; difference between the satellite measurements and model simulations for CTL (c) and E10 (e). SCIAMACHY δD data is systematically decreased by 20 ‰.

Figure 2: Same as Figure 1, but for TES mid-tropospheric (800 to 500 hPa pressure) observation. TES δD data is systematically increased by 20 ‰. TES's averaging kernel is applied to each collocated IsoGSM data.

Figure 3: Zonal (a-c) and meridional (d-f) averages of modeled (CTL is red and E10 is blue) and observed (black) δD in atmospheric column vapor by SCIAMACHY. The zonal averages (a to c) are for all longitudes, whereas the meridional averages are for the tropical regions (equatorward of 30°). The top panels (a and d) represent annual climatology, the middle panels (b and e) are for JJA means, and the bottom panels (c and f) are for DJF means.

Figure 4: Similar to Figure 3, but for the TES mid-tropospheric δD . For reference, the IsoGSM results without TES's averaging kernel ("noak") are shown by orange and sky blue dashed lines for CTL and E10 experiments, respectively.

Figure 5: Scatter diagrams between the satellites' observations and the IsoGSM E10 simulation climatology covering 45°S-45°N. (a) to (c) are SCIAMACHY data, and (d) to (f) are TES data. (a) and (d) are for annual average, (b) and (e) are for JJA, and (c) and (f) are for DJF. Contours indicate relative frequency of the two-dimensional histograms with a contour interval of 0.5% and a class range of 10‰ for each axis.

Figure 6: Scatter diagrams between vapor δD and humidity in bi-logarithm expression. (a) to (c) use the satellite observation climatology, and (d) to (f) use IsoGSM E10 simulation climatology. Blue and red dots represent SCIAMACHY and TES observations (or collocations), respectively. (a) and (d) are for annual average, (b) and (e) are for JJA, (c) and (f) are for DJF. The black solid lines indicate the Rayleigh-type fractionation, where heavy isotopes are preferably removed from vapor by condensation, starting from three typical vapors originating from the sea with 5°C, 15°C, and 25°C. The black dashed lines indicate so-called "mixing lines", which represent the mixing of two isotopically distinctive air masses (-350‰ and -80‰) starting with three different vapor amount (VMR) of 0.07 0.15 0.30‰v) for the depleted air mass.

Figure 7: Global distribution of δD seasonal variations using SCIAMACHY data (black lines) and two IsoGSM simulations (green dotted lines for CTL and red dashed lines for E10).

Figure 8: Same as Figure 7, but for TES mid-tropospheric data.

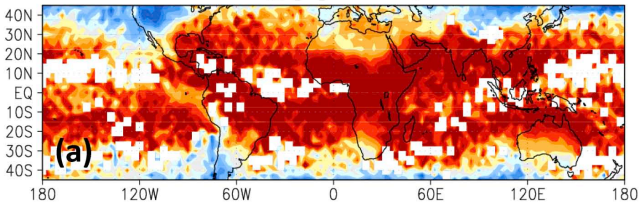
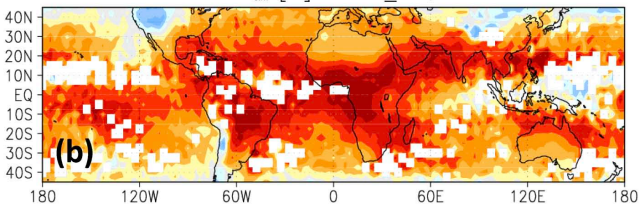
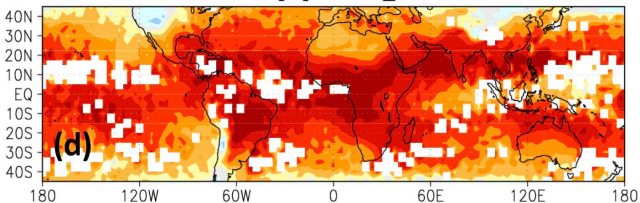
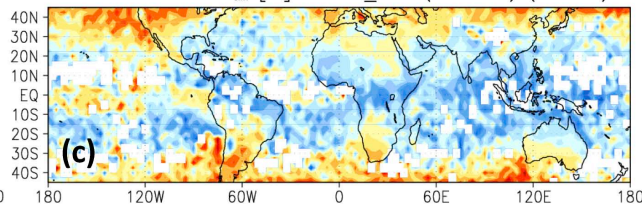
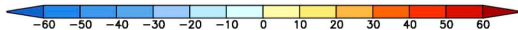
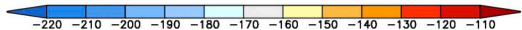
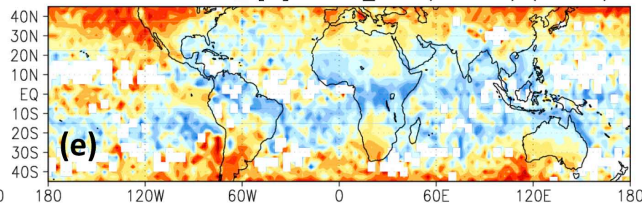
Figure 9: Comparison of the snapshot measurements with the simulation at a grid of 15°E and 20°N. δD of atmospheric column vapor is shown at the top (a and b), and the amount of total precipitable water (TPW) is shown at the bottom (c and d). Time series are on the left (a and c), and scatter plots are on the right (b and d). In the left-hand panels, red circles and blue lines represent SCIAMACHY and the IsoGSM E10 simulation, respectively, while the small red dots are from SCIAMACHY single measurements before averaging for 6-hour and 2.5°x2.5° space.

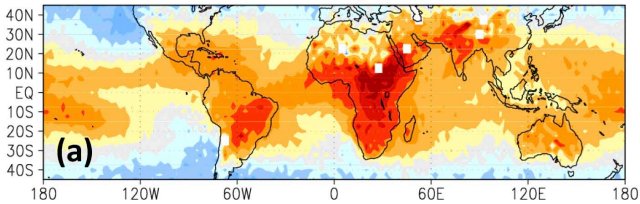
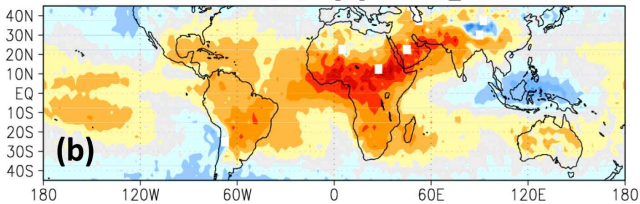
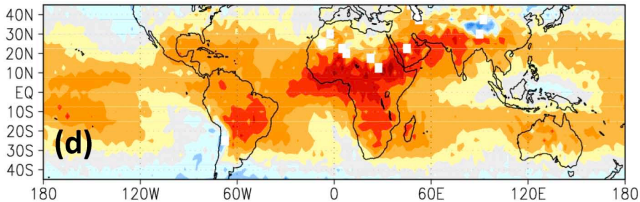
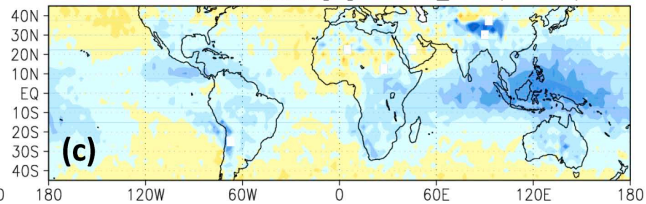
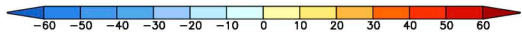
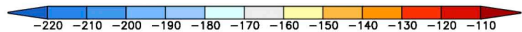
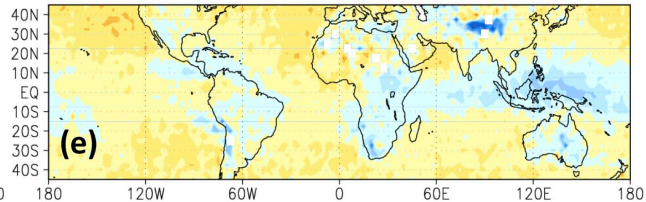
Figure 10: Similar to Figure 9, but for TES mid-tropospheric data at 67.5°E and 25°N. Unlike Figure 9, there is no small red dot and each red circle represents a single measurement by

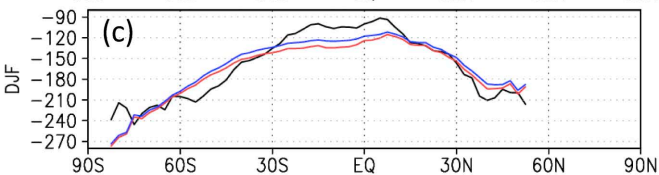
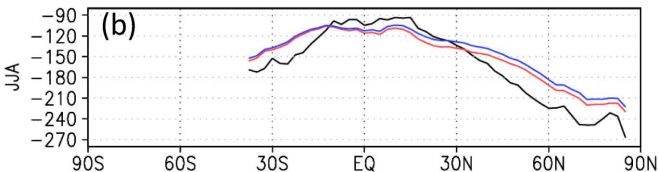
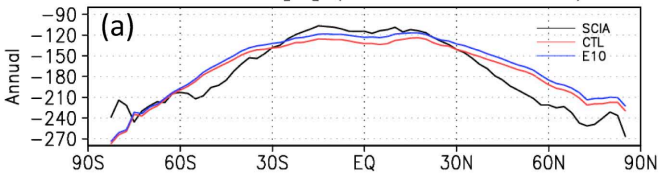
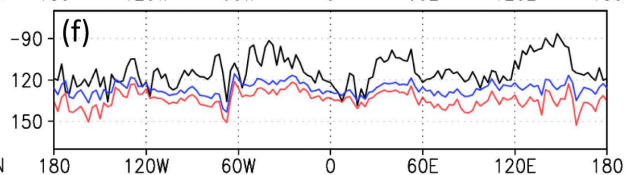
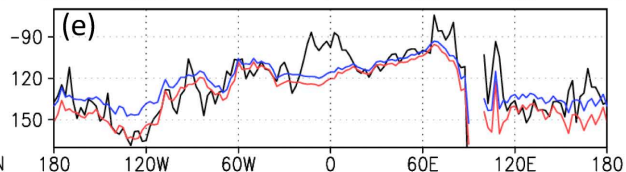
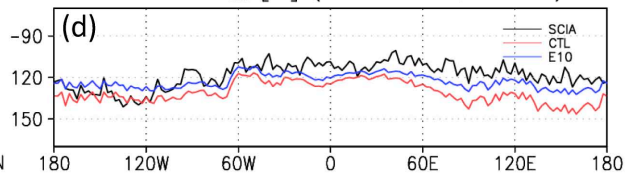
TES. The 6-hourly IsoGSM simulation results without AK application are shown by sky blue lines.

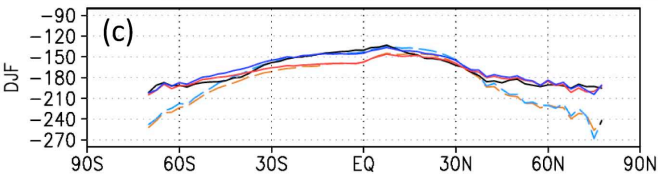
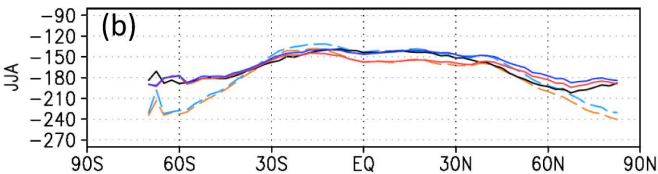
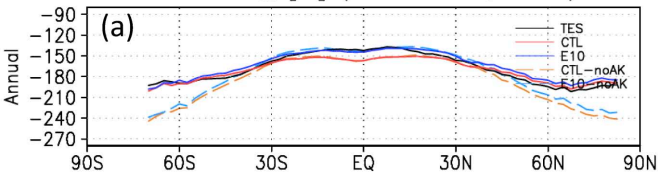
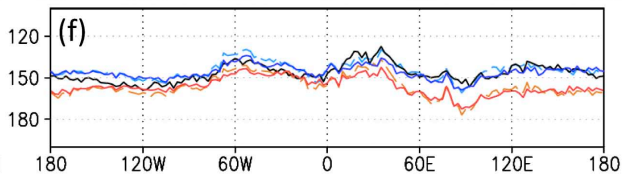
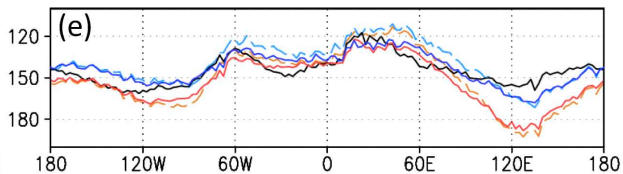
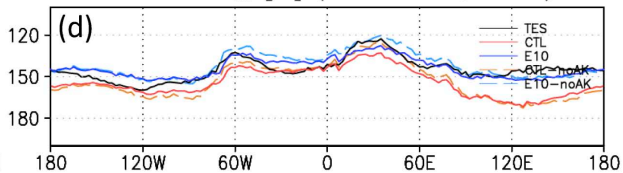
Figure 11: Global distribution maps of correlation coefficients between the time series of the SCIAMACHY or TES observations and the IsoGSM E10 simulation; (a) SCIAMACHY atmospheric column δD , (b) SCIAMACHY total precipitable water, (c) TES mid-tropospheric δD , and (d) TES mid-tropospheric volume mixing ratio. Gray areas indicate that there are not enough number of data for valid regression. "X" and "Y" indicate the approximate locations of the grids for Figure 9 and Figure 10, respectively.

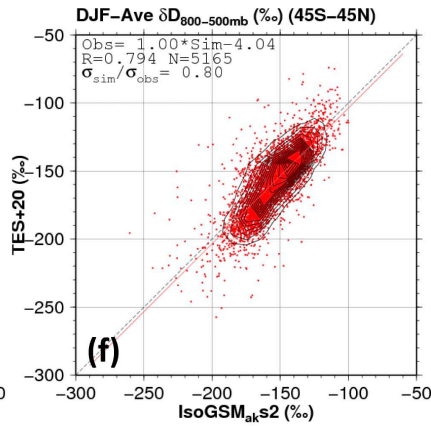
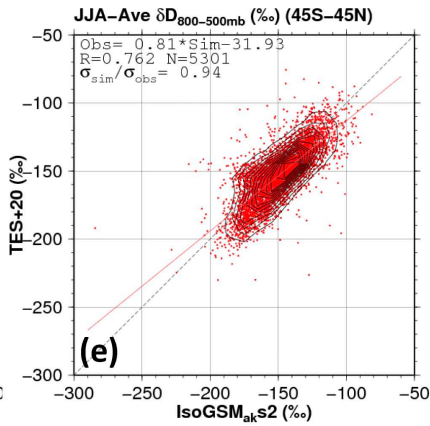
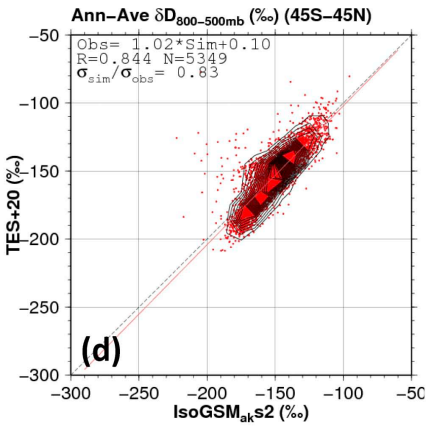
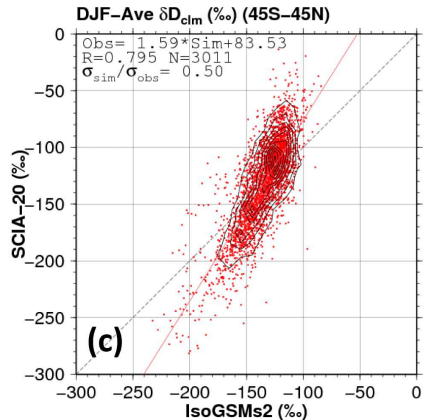
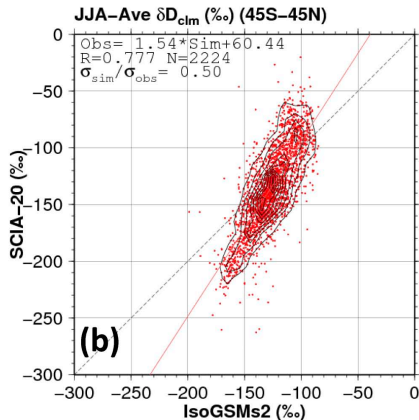
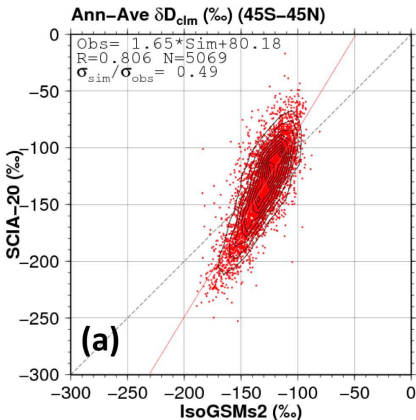
Figure 12: Similar to Figure 11, but for slope of the linearly regressed relationship.

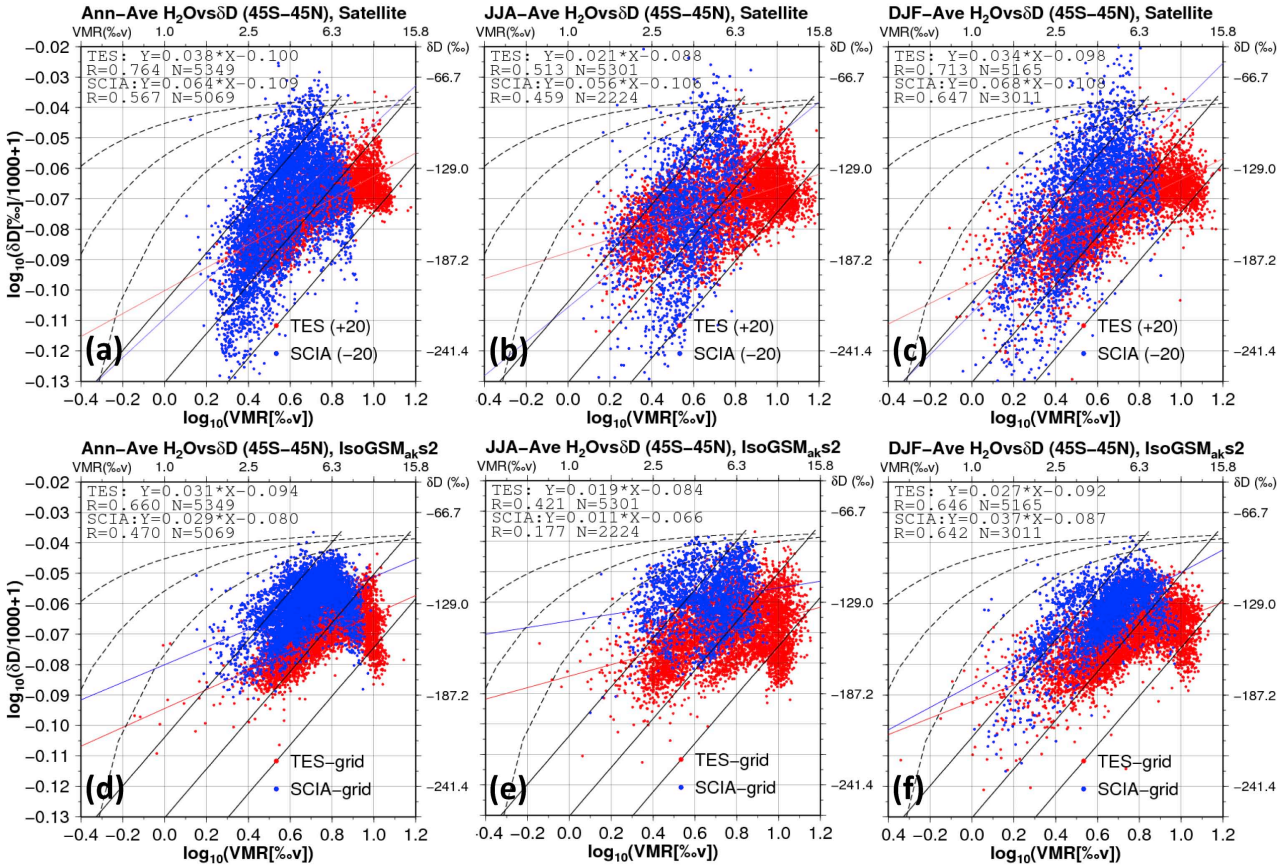
AnnAve δD_{clm} [‰] SCIA-20, N>=10AnnAve δD_{clm} [‰] IsoGSM_CTL, N>=10AnnAve δD_{clm} [‰] IsoGSM_E10, N>=10AnnAve Diff in δD_{clm} [‰] IsoGSM_CTL-(SCIA-20) (N>=10)AnnAve Diff in δD_{clm} [‰] IsoGSM_E10-(SCIA-20) (N>=10)

AnnAve $\delta D_{800-500mb}$ [‰] TES+20AnnAve $\delta D_{800-500mb}$ [‰] IsoGSM_{ok}_CTLAnnAve $\delta D_{800-500mb}$ [‰] IsoGSM_{ok}_E10AnnAve Diff in $\delta D_{800-500mb}$ [‰] IsoGSM_{ok}_CTL-(TES+20)AnnAve Diff in $\delta D_{800-500mb}$ [‰] IsoGSM_{ok}_E10-(TES+20)

ZnIAve δD_{clim} [‰] (Offset: -20‰, N \geq 10)MrdnIAve δD_{clim} [‰] (Offset: -20‰, N \geq 10)

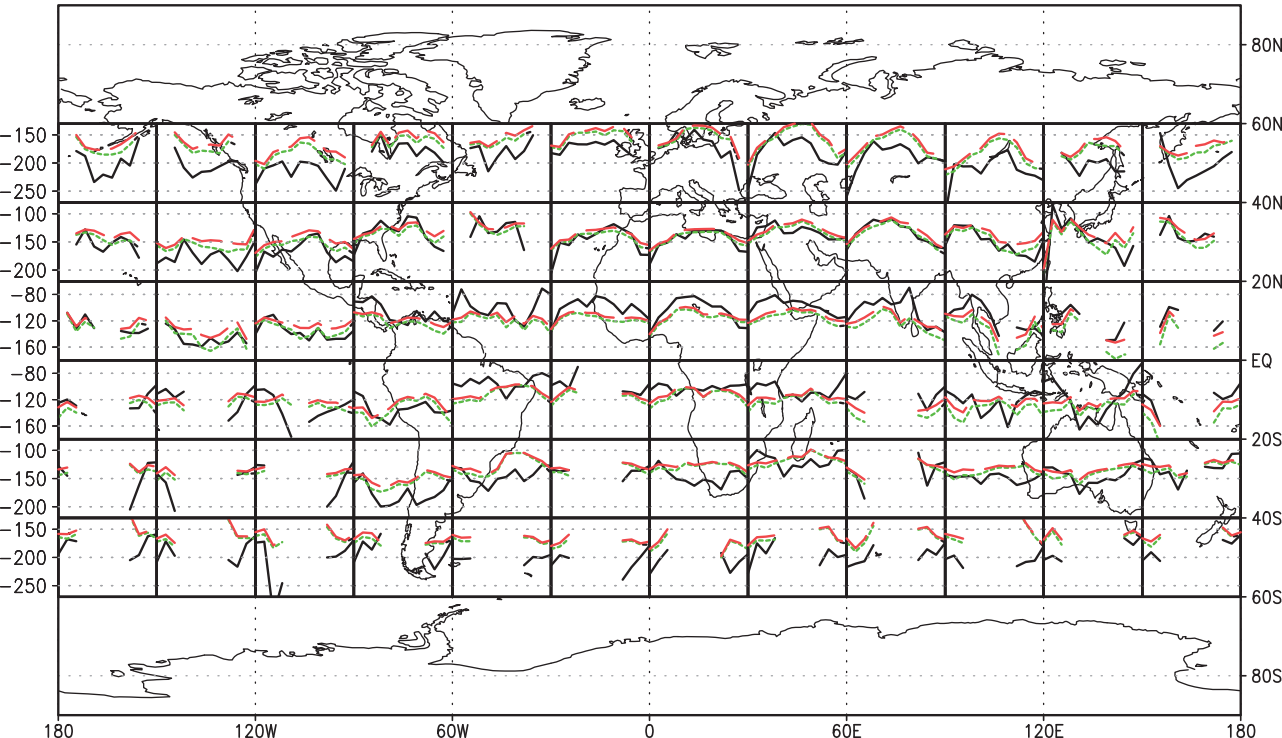
ZnIAve δD_{clm} [‰] (Offset: +20‰, N \geq 1)MrdnlAve δD_{clm} [‰] (Offset: +20‰, N \geq 1)





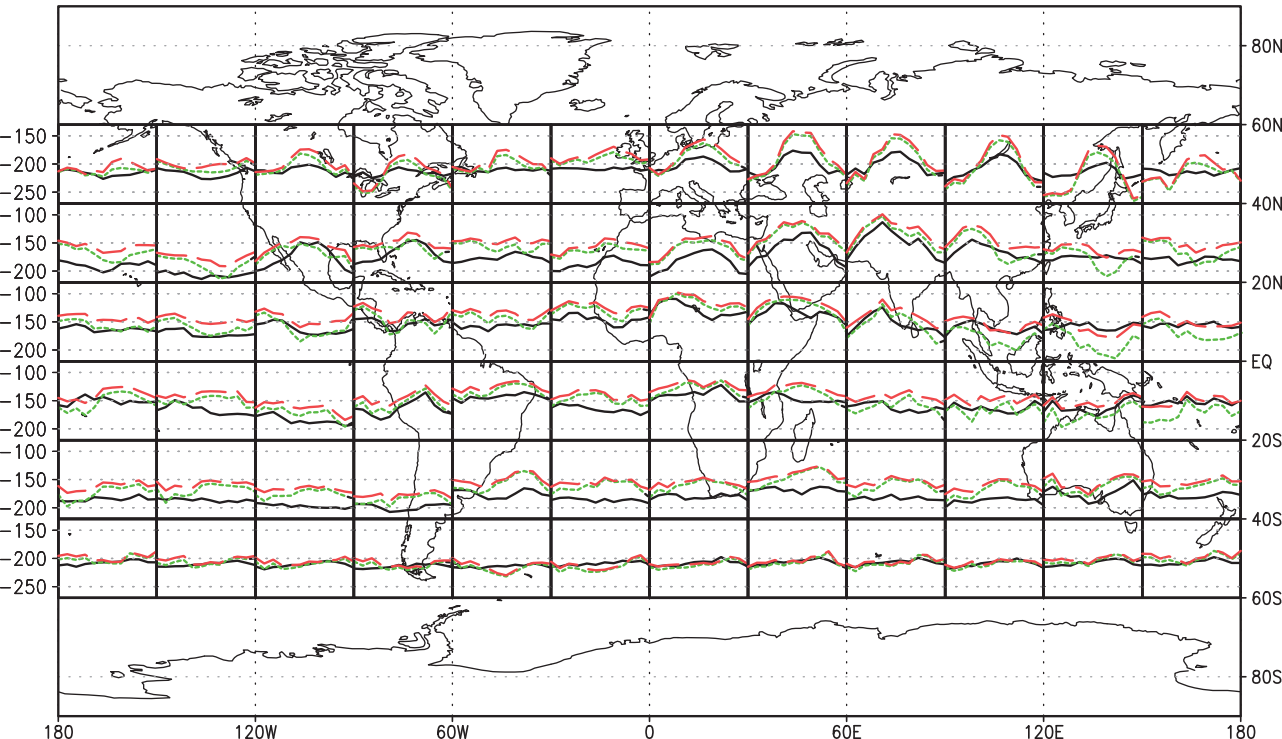
SCIA-20 & IsoGSM CTL/E10 δD_{clm} [‰] (N >= 10)

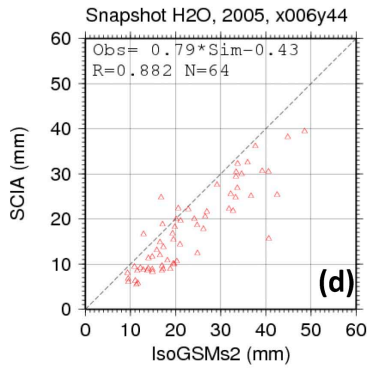
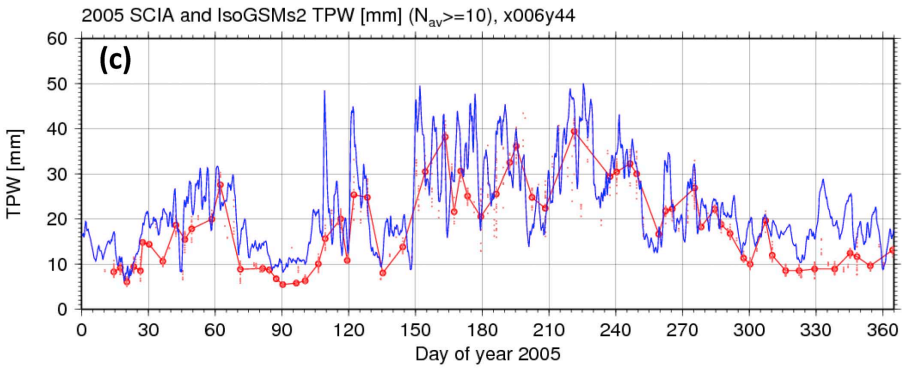
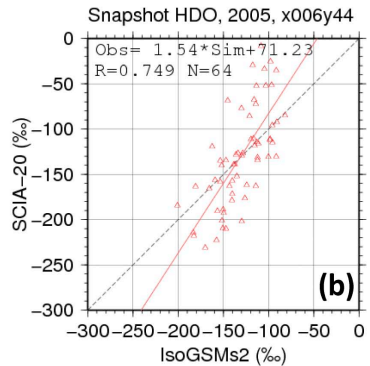
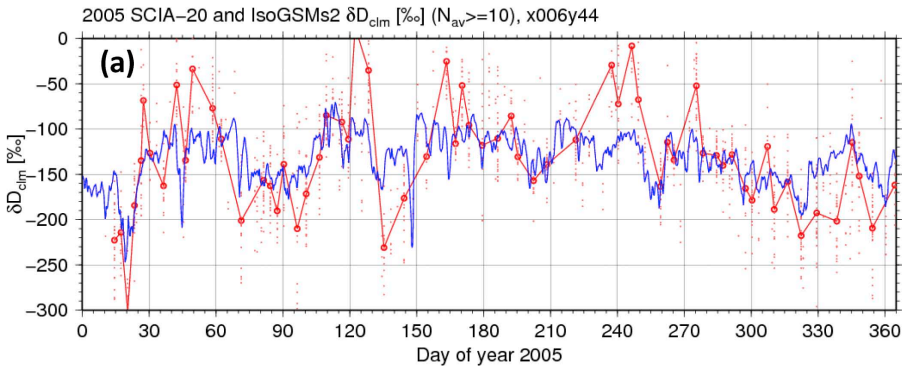
- SCIA
- - - CTL
- - - E10

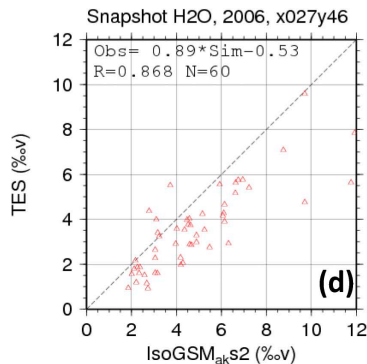
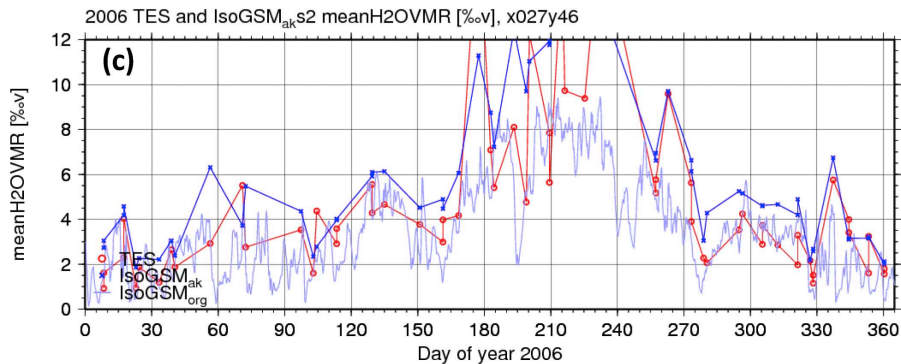
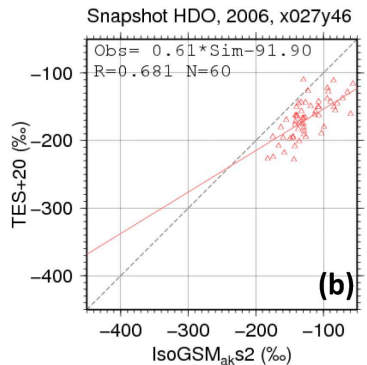
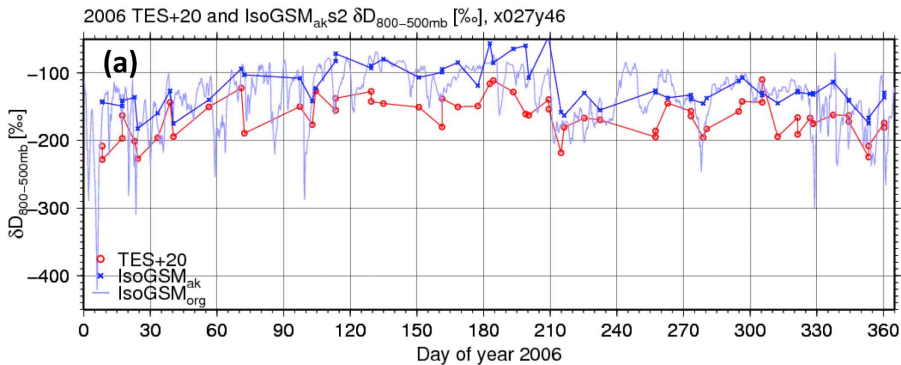


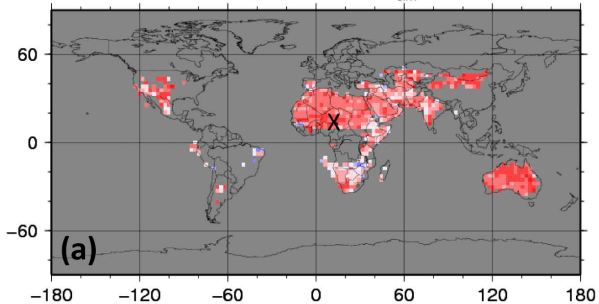
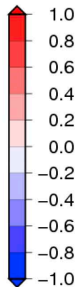
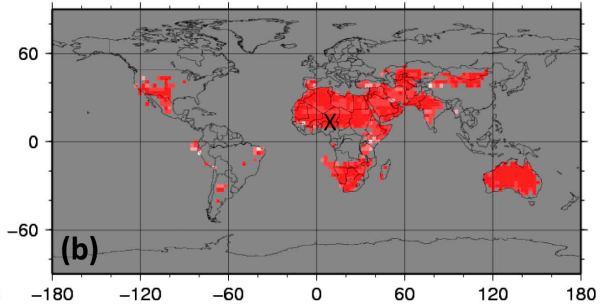
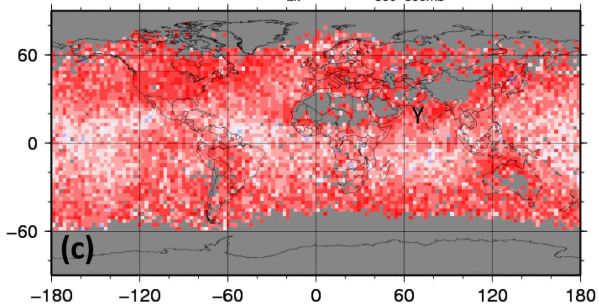
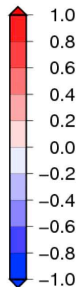
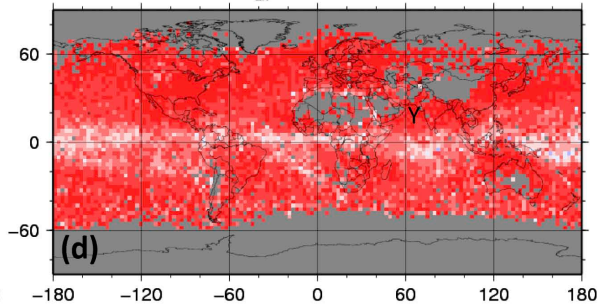
TES+20 & IsoGSM_{ak} CTL/E10 $\delta D_{800-500mb}$ [%]

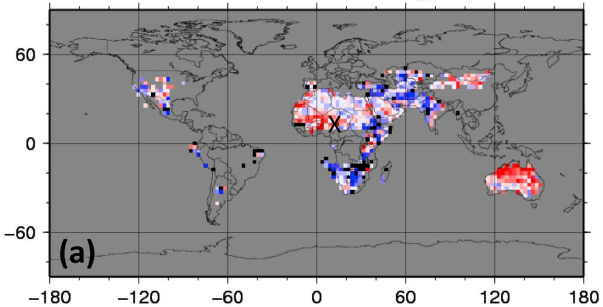
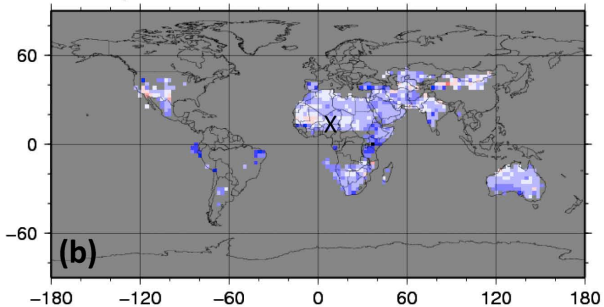
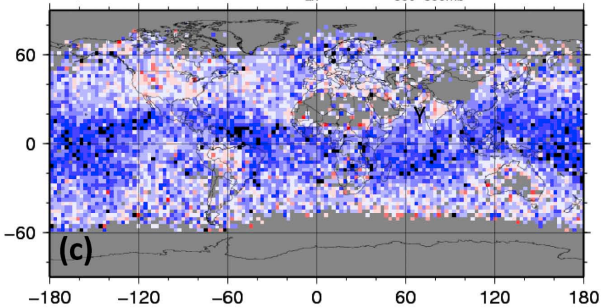
— TES
- - - CTL
- - - E10







R b/w SCIA-20 vs IsoGSMs2 for δD_{clm} , $N \geq 10$, 2005R b/w SCIA vs IsoGSMs2 for TPW, $N \geq 10$, 2005R b/w TES+20 vs IsoGSM_{ak}s2 for $\delta D_{800-500\text{mb}}$, $N \geq 10$, 2006R b/w TES vs IsoGSM_{ak}s2 for meanH2OVMR, $N \geq 10$, 2006

Slope b/w SCIA-20 vs IsoGSMs2 for δD_{clm} , $N \geq 10$, 2005Slope b/w SCIA vs IsoGSMs2 for TPW, $N \geq 10$, 2005Slope b/w TES+20 vs IsoGSM_{ak}s2 for $\delta D_{800-500\text{mb}}$, $N \geq 10$, 2006Slope b/w TES vs IsoGSM_{ak}s2 for meanH2OVMR, $N \geq 10$, 2006